Journal of Materials Chemistry B

Accepted Manuscript

ROYAL SOCIETY OF CHEMISTRY

www.rsc.org/materialsB

Journal of Materials Chemistry B

Dynamic Article Links ►

Cite this: DOI: 10.1039/c0xx00000x

ARTICLE TYPE

www.rsc.org/xxxxxx

Novel multifunctional PB and PBH hydrogels as soft filler for tissue engineering

Xian Li,[1§] Wenjiao Xue,[2§] Yannan Liu,[1] Daidi Fan,[*1] Chenhui Zhu,[1] and Xiaoxuan Ma[1]

Received (in XXX, XXX) Xth XXXXXXXXX 20XX, Accepted Xth XXXXXXXXX 20XX

DOI: 10.1039/b000000x

In this study, we designed multifunctionalized hydrogel scaffolds and injectable particles based on high-molecular-weight (MW) pullulan and human-like collagen (HLC) crosslinked with 1, 4-butanediol diglycidyl ether (BDDE) for combination therapy tissue restoration. The properties of the pullulan/BDDE (PB) and pullulan/BDDE/human-like collagen (PBH) hydrogels were characterized via swelling ratio measurements, mechanical tests, and enzymatic degradation *in vitro* and via subcutaneous injections *in vivo*. The results demonstrate that the dry hydrogels completely returned to their original state in deionized water. The elastic modulus of the PBH53 dry hydrogels is higher than that of the other hydrogels after exposure to bending stress and compression stress, with a maximum value of 7858.93 MPa. In addition, the *in vitro* live/dead staining and cell adhesion of the PBH hydrogels were exhibited superior fibroblast morphology without high levels of cell death much better than those of the PB hydrogels. *In vivo*, PB and PBH particles with good biocompatibility and anti-biodegradation were successfully prepared via granulation of wet PB and PBH hydrogels for efficient subcutaneous injection in Kunming mice and New Zealand rabbits. Therefore, the PB and PBH hydrogels were found to be acceptable, safe, soft materials for use in skin restoration, cartilage treatment, and lacrimal dryness therapy.

Keywords: collagen/pullulan hydrogels, pullulan hydrogels, BDDE, soft filler, cartilage

1. Introduction

The design and development of hydrogels with functional characteristics and high molecular weight are crucial for successful tissue restoration. Generally, hydrogels are used for tissue engineering, drug delivery, gene delivery and wound healing, [1] while functional hydrogels, as soft materials, are used for skin tissue restoration and cartilage tissue engineering and even as potential replacements for lacrimal artificial canals to treat lacrimal dryness. Therefore, functional hydrogels with tailored compositions and improved properties can promote injection efficiency and can achieve higher mechanical strength in numerous therapies.

Natural polysaccharides are highly suitable candidates for the design of novel biomaterials because they are renewable, non-toxic, biodegradable materials. [1] Numerous studies have focused on the use of polysaccharides, such as chitin, [2] chitosan, [3] heparin, [4] alginate, [5] and pullulan, [6] for biomedical applications. Pullulan is used as a diffused biomaterial in tissue engineering due to its non-ionic exopolysaccharide of fungal origin and its non-toxic, non-immunogenic, non-carcinogenic nature. Indeed, pullulan has been widely used for gene therapy, [7] drug release, [6] bone tissue engineering, [8] and therapy against hepatocellular carcinoma. [9] Additionally, some researchers have used pullulan in the development of scaffolds for tissue restoration. Jelly-like hydrogels substituted for cartilage in bone tissue engineering have become increasingly popular to address limitations in tissue grafting for a wide variety of diseases including osteoarticular pathologies. [8] Therefore, we prepared ready-to-use hydrogels that can be easily produced in various shapes and sizes for different clinical applications and that can generate bone for substantial-sized defects. Clinically, the application of pure pullulan is difficult in normalization treatments. To overcome this drawback, a crosslinking agent is necessary in the copolymer system.

Recently, human-like collagen (HLC) and its relevant composite materials, including vascular scaffolds, [10] artificial bones, [11] chelated products [12] and hydrogels, [13] have been introduced and are acceptable for clinical use. Therefore, the efficiency of skin tissue therapies can be enhanced by optimizing the pullulan/HLC composition. HLC in hydrogel systems can be effective against most collagen loss from skin or bone due to aging. Some

investigations have already demonstrated the potential advantages of this approach for filler treatment and bone therapy. Therefore, in this study, we designed a pullulan-based carrier system modified with HLC, using BDDE as a crosslinking agent for the composite, to fabricate functional materials for skin restoration, cartilage treatment, and lacrimal dryness therapy.

These hydrogel systems use high-molecular-weight pullulan (100,000 to 530,000 g/mol) in a conjugate composition combined with a crosslinker. However, a different hydrogel system is preferred when distinct types of biomacromolecules are to be crosslinked, especially if the lateral composites involved are also different. The resulting overall amide group thus gains increased mobility with the amino group of the side chain functional groups of the HLC backbone via the crosslinker. Several types of crosslinkers have been reported, such as glyoxal [14] and dimethyl suberimidate, [15] but the classical 1, 4-butanediol-diglycidyl ether (BDDE) is still in use and meet the FDA/EMEA regulations. BDDE acts as a phase-transfer catalyst [16] at the interface between the crosslinker dispersion droplets and the highly hydrated biomacromolecules in a colloidal state. The crosslinking sites of BDDE are the free amino and hydroxyl groups, and the crosslinking process is carried out under alkaline conditions. [17]

In this work, pure pullulan and an HLC-pullulan composition generated by crosslinking with BDDE were investigated. The mechanical strength, swelling behavior, biodegradation and cell adhesion parameters were evaluated for the two types of hydrogels (PB and PBH hydrogels). Specifically, the effects of the higher molecule weight of pullulan and modification by HLC to induce chemical gelation were investigated. Additionally, the effects of the two types of hydrogel particles on biodegradation and inflammation were studied; it was found that the PB and PBH hydrogels, as soft materials, are suitable for tissue engineering. This study presents novel findings, as this is the first report on the functional character of hydrogels composed of HLC and high-MW pullulan, using BDDE as a crosslinker.

2. Methods/Experimental

2.1 Materials and methods

HLC was expressed in *E. coli* from a cloned partial cDNA derived from human collagen mRNA. HLC is a macromolecular water-soluble protein with a molecular weight of 97,000 (China patent number: ZL01106757.8). Pullulan (MW, 100,000 g/mol; 530,000 g/mol) was produced at the synthesis laboratory of the Shannxi Provincial Institute of Microbiology. 1, 4-butanediol diglycidyl ether (BDDE) and the live/dead viability/cytotoxicity kit were purchased from Sigma-Aldrich. DMEM medium and fetal bovine serums (FBS) were obtained from Hyclone (Logan, UT, USA). All solvents and reagents were analytical grade.

2.2 Synthesis of PB and PBH hydrogels

For the preparation of PB hydrogels (PB10 and PB53) via chemical crosslinking, we mixed an aqueous solution of pullulan (MW: 100,000 g/mol (P10) and 530,000 g/mol (P53)) with 0.1 mL of 1, 4-butanediol diglycidyl ether (BDDE) under alkaline conditions. For the pullulan solution, 1 g of pullulan was dissolved in 10 mL of sterile pyrogen-free water. The mixture was stirred for 30 min at room temperature until a transparent viscous liquid was produced. This transparent viscous liquid then underwent a sol-gel transition at 50°C in a water bath for 3 h.

Synthesis of the PBH hydrogel (PBH10 and PBH53) involved a human-like collagen polymer and pullulan (P10 and P53). For the polymer, 0.2 g of human-like collagen was dissolved in 10 mL of sterile pyrogen-free water, and 1 g of pullulan (P10 and P53) was added with stirring. The pH was adjusted to 8.0 using 0.1 M NaOH. The BDDE solution (0.1 mL) was added to the resultant solution with stirring for 30 min at room temperature, to produce a viscous liquid. This viscous liquid then underwent a sol-gel transition at 50°C in a water bath for 3 h.

The residual BDDE was removed as follows: yellow-colored PB and PBH hydrogels were removed from the water bath and wrapped with medical gauze in a container over a hot bath with sterile pyrogen-free water and a magnetic stirrer for 72 h. The sterile pyrogen-free water was refreshed every two hours. Finally, the yellow-colored PB hydrogels became transparent, and the yellow-colored PBH hydrogels changed to oyster white. Half of the hydrogels (PB and PBH) were cut into cylindrical hydrogels with a diameter of 10 mm and a height of 10 mm or a diameter of 10 mm and a height of 3 mm for further analysis. The mechanical strength, swelling behavior, internal aperture, cell adhesion and enzyme degradation were evaluated after further washing of the hydrogels for 24 h, and the PBS was changed to wash for another 6 h. The remaining hydrogels (PB and PBH) were converted into particles (micron-level grain) using a granulator. The particles were poured into 50-μm white polyester fabrics for further washing for 24 h and were washed again for another 6 hours after changing the PBS. Next, the particles were distilled for 20 min at 121°C three times. Finally, the particles were stored in a refrigerator at 4°C for further investigation, for example, for the composition of hydrogels, morphology of particle after distillation, for determining the residual amount of BDDE in the PB and PBH hydrogels and for subcutaneous injection into animals (adult male Kunming mice and adult male New Zealand rabbits).

2.3 Fourier transforms infrared spectroscopy (FT-IR)

FT-IR spectra of HLC, pullulan (P10 and P53), BDDE, PB hydrogels (PB10 and PB53) and PBH hydrogels (PBH10 and PBH53) were recorded using a PerkinElmer Spectrum 2000 spectrometer (PerkinElmer Instruments, Inc.) in the range of 4000–600 cm^{-1}. Each spectrum was taken as the average of 16 scans at a resolution of 4 cm^{-1}.

2.4 Residual BDDE in the PB and PBH hydrogels

Approximately 0.6 g of the PB and PBH hydrogels was enzyme-reacted with 1 mL of pullulanase (1000 ASPu/g) for 24 h at 37°C in a water bath shaker, a speed of 70 rpm. The hydrogel enzymolysis liquid was filtered to test for residual BDDE. Standard BDDE solutions were prepared at concentrations of 8.0 μg/g, 4.0 μg/g, 2.0 μg/g, 1.0 μg/g, 0.5 μg/g and 0.25 μg/g. Then, 200 μL of various concentrations of standard BDDE and hydrogel enzymolysis liquid was added to 100 μL, 125 mmol/L nicotinamide for 120 min at 37°C. Next, 1 mL of 15% acetophenone and 1 mL of 1 mol/L KOH solution was added to the above solution for 10 min in an ice bath. Finally, 5 mL of methanoic acid was added for 5 min at 60°C, and the mixture was transferred to an ice bath. The following solution was maintained at room temperature for 10-15 min, and fluorescence

measurements were obtained using a fluorescence spectrophotometer, with excitation and emission wavelengths of 380 and 435 nm, respectively.

2.5 Physical characterizations of the hydrogels

Hydrogel disks were dehydrated using lyophilization to assess the swelling behavior and to obtain scanning electron microscopy (SEM) images. For SEM, cross-sections of the hydrogel cylinders and the particles were carefully lyophilized to maintain their three-dimensional porous structures. The lyophilized samples were immersed in liquid nitrogen, and the vitrified samples were carefully cut with a cold knife. The cut samples were mounted, sputter-coated with gold, and observed under using a Hitachi S-570 SEM (Hitachi, Tokyo, Japan).

To measure the equilibrium swelling ratio, fully swollen hydrogel samples were weighed after excess surface water was gently removed by blotting with Kimwipes, freeze-dried and weighed again. Each measurement was repeated at least three times. The swelling ratio was determined according to the following equation: Swelling Ratio = $(W_s - W_d)/W_d$, where W_s is the weight of the swollen gel and W_d is the weight of the freeze-dried gel, respectively. For incubation studies, dry PB and PBH hydrogels were incubated in deionized water at 37°C. The hydrogel diameter and height were measured at 1 h, 12 h, 24 h, 48 h, 72 h, and 96 h. Six samples were tested for each condition.

The mechanical properties of the hydrogels: the compression stress of wet and dry hydrogels and bending stress of dry hydrogels (10-mm diameter and 10-mm height) were evaluated using a gel strength instrument (Electronic Universal Testing Machine). The compression speed was adjusted to 2 mm/min. The elastic modulus, the relationship between the compression load and compression displacement, the bending stress and compression displacement were determined.

2.6 *In vitro* degradation

After distillation, dry PB and PBH hydrogels (10-mm diameter and 3-mm height) were incubated with pullulanase (20 U/mL) in PBS and weighed weekly. A similar experiment was performed with collagenase I (20 U/mL) in PBS. Combination degradation studies using both pullulanase and collagenase I was conducted in PBS using the same concentrations as above. The initial weight at time 0 was the dry weight of the hydrogels (W_0), and after being degraded by the enzymes, the wet hydrogels were washed three times by water before vacuum drying (W_1). These hydrogels were used for subsequent measurements. The weight loss (%) was calculated as follows: $(W_0-W_1)/W_0\times100\%$. Experiments were performed six times for each condition at 37°C.

2.7 Cell adhesion and live/dead staining

Cell viability was evaluated by cell adhesion and live/dead staining was observed using a confocal microscopy and SEM, respectively. The live/dead viability/cytotoxicity kit for mammalian cells are using for live/dead staining as described previously.[18] Cryopreserved fibroblasts were thawed, centrifuged, and then cultured in DMEM containing 10% FBS. Confluent cells were passaged into multiple flasks for subsequent experiments. One day before culture, four wet hydrogel samples (10-mm diameter and 3-mm height) were sterilized at 121°C for 5 min, rinsed with DMEM twice in a 48-well plate, and then equilibrated in the medium overnight until cell plating. For surface adhesion studies, logarithmic-phase fibroblasts (5×10^5 cells/mL) were seeded onto four hydrogels, and 1 mL of DMEM was added to each well in a 5% CO_2, 37°C incubator. Parts of the samples were fixed in glutaraldehyde at 24, 48 and 72 h, and the cell morphology was observed by SEM after vacuum freeze drying. The remaining portions of the samples were stained by live/dead staining at 24 and 72 h to evaluate cell viability on the hydrogels, and the live/dead cells were observed using a confocal microscopy. The death rate of cell was calculated by dead cell/live cell×100%. The cell viability was calculated by (1-death rate of cell). A control condition is conducted in normal fibroblast cultured by DMEM media, the test samples were cultured by the PB10, PBH10, PB53, PBH53 hydrogels. Five parallel samples of each material were utilized.

2.8 Animal experiments

All experiments were performed in compliance with the relevant laws and institutional guidelines, and conducted with the approval of the Institute Animal Ethics Committee. This study was supported by Shaanxi Key Laboratory of Degradable Biomedical Materials and Northwest University. A total of 36 adult male Kunming mice and 36 adult male New Zealand rabbits were quarantined for a week, with free access to food and water but without antibiotics. After 2 weeks, healthy Kunming mice and New Zealand rabbits were used for the injections. After shaving and disinfection, 0.2 mL and 0.5 mL of particles and physiological saline (as control group) were subcutaneously injected into the back of the Kunming mice and New Zealand rabbits, respectively. The biocompatibility of the hydrogels *in vivo* under physiological conditions was evaluated on different parts of the back of the Kunming mice and New Zealand rabbits. For the Kunming mice, two areas were chosen for injection. For the New Zealand rabbits, eight areas were chosen for injection. After 1 and 24 weeks, the mice and rabbits were euthanized by carbon dioxide inhalation, and whole tissue samples including the skin and the particles were isolated. Then, 1-cm-thick isolated tissue samples were fixed in 10% neutral buffered formalin for H&E staining, and 1-mm^3 tissue samples were fixed in 2.5% glutaraldehyde (including 0.1 M PBS and 4% paraformaldehyde) for transmission electron microscopy (TEM) analysis.

2.9 H&E staining

The fixed tissues were dehydrated through a graded ethanol series (30%, 50%, 70%, 80%, 90%, 95%, and 100%), immersed in liquid wax and then embedded in epoxy resin. Tissue blocks were sectioned using a Leica RM2016 diamond saw microtome (Leica Instruments Ltd, Germany) with a tissue thickness of 5 μm and collected on coated slides. The samples were prepared for histopathological analysis using hematoxylin and eosin (H&E) staining. The samples were then rinsed three times in PBS and incubated in a 4% diaminobenzidine substrate solution at room temperature. Images were acquired using an optical microscope connected to a CCD camera (DP25, Olympus, Japan).

2.10 Transmission electron microscopy (TEM) analysis

Harvested tissue samples (epidermis and dermis) with a volume of 1 mm^3 were immediately fixed with 2.5% phosphate-buffered glutaraldehyde (1 M phosphate-buffered solution and 4% paraformaldehyde) for 2 h, rinsed with 0.1 M PBS for 30 min, post-fixed in 1% osmium tetroxide for 2 h, and finally rinsed for 10 min using a 0.1 M phosphate buffer. The samples were

subjected to an ethanol series (30, 50 and 70%) for 10 min at each concentration and were stained in a 70% ethanol solution of uranylacetate for 2 h. Next, the samples were dehydrated with 90% (2, 3 and 10 min) and then 100% (3, 3 and 10 min) ethanol and displaced with epoxyethane. Finally, the samples were embedded in Epon 812. Semi-thin sections (1-2 μm) were cut and stained with methylthioninium chloride to select appropriate areas for observation. Ultrathin sections (50-70 nm) were stained with 4% uranyl acetate and 0.5% lead citrate and observed by TEM (HITACHI, H-600, Japan).

2.11 Calculations and data analysis

The data were collected in a Microsoft Excel 2000 database, and the results are presented as mean values and standard deviations using Origins 7.0 software. Student's *t*-test was performed to determine the statistical significance between experimental groups. A value of $p < 0.05$ was considered to be statistically significant.

3. Results and Discussion

3.1 Network formation

Fig. 1 (A) shows the FT-IR spectra of HLC, pullulan (P10 and P53), BDDE, and the corresponding hydrogels (PB and PBH). For all of the spectra, the peaks at 905±5 cm^{-1} and 1022±5 cm^{-1} are attributed to the vibrational modes of the saccharide units, [19] while the peak at 1159±5 cm^{-1} is related to –CHOH in the PB and PBH hydrogels. The secondary alcohols primarily arise from the epoxidation reaction between the saccharide units and the BDDE (Fig. 1B). In this reaction, the alkylene oxides of BDDE must be opened via a concerted process and react with the $–CH_2OH$ of the pullulan under alkaline conditions. The primary differences among the spectra are found in the 1450 to 1700 cm^{-1} region. Peaks at 1459 cm^{-1}, 1510 cm^{-1} and 1645 cm^{-1} are present in the PBH hydrogel spectrum and are related to the –RCONHR' due to HLC and pullulan crosslinking via BDDE (Fig. 1 B). After BDDE crosslinking, the primary amino groups in the HLC decrease in number, and secondary amides are formed. Indeed, the peak at 1510 cm^{-1} decreases in intensity in the spectrum of the PBH hydrogels, while the intensity of a peak at 1646 cm^{-1} (amide type II) increases. The spectra of the PBH hydrogels is show a drastic increase in intensity in the region near 1459 cm^{-1}, which corresponds to the C-N stretching vibration, thus confirming the presence of amide type II in the PBH hydrogels. Because amide bonds are also found in this region, crosslinking of the PB hydrogels may have contributed to the peaks at 1646 cm^{-1} and 1650 cm^{-1}, which may be related to -C=O stretching.

Fig.1

Fig. 1. (A) FT-IR spectra of P10, P53, HLC, BDDE, PB10, PBH10, PB53 and PBH53. (B) Proposed mechanisms for interactions among pullulan, HLC and BDDE: the reaction among pullulan, HLC and BDDE in a hot bath at 50°C under alkaline conditions.

3.2 Hydrogel preparation and characterization

Hydrogels were crosslinked via BDDE using pullulan of different molecular weights and HLC as functional materials. Pullulan and HLC monomers were used in the pre-polymerization solution to create each hydrogel sample. Purified hydrogels kept in deionized water were then removed to investigate the morphology by visual observation. Fig. 2 shows sample images of the wet and dry hydrogels. The PB hydrogel is a jelly-like hyaline (Fig. 2 A and C), and the PBH hydrogels are milk-white and jelly-like (Fig. 2 B and D); the sample resembles a white cylindrical artificial bone during the freeze-drying process (Fig. 2 E). The swelling ratio, [20] length and diameter of the hydrogels were measured over time as they re-dissolved in deionized water (Fig. 2 E1, F1 and G1). Kinetic studies revealed that the hydrogels swelled rapidly, reaching equilibrium within 48 h. The composite PBH hydrogels showed less swelling compared to the PB hydrogels.

The swelling extent was found to decrease with the amount of HLC used for the reaction, particularly for the PB and PBH hydrogels with higher-molecular-weight pullulan. For MWs from 100,000 g/mol to 530, 000 g/mol, the swelling ratios decreased from 10.97 to 10.35 g/g and 9.84 to 9.2 g/g, respectively, at 96 h. Interestingly, the lengths and diameters of the hydrogels changed over time, decreasing and then increasing, until the initial form was restored (Fig. 2 E, F and G). The initial length and diameter were obtained after dissolution for 96 h (Fig. 2 F1 and G1). Hydrogel particles were obtained using a granulator, followed by three steps of distillation (Fig. 2 H1). Because the residual BDDE in the hydrogels is lower than the standard amount of residual BDDE (2 vg/mL), these hydrogels can be injected *in vivo*. Therefore, the PB and PBH hydrogels may be promising as soft fillers and cartilage for tissue engineering.

All hydrogels exhibited a homogenous, porous structure, with differences only in their distribution and pore size (Fig. 3 A, B: cross-section). A maximum size of approximately 50-80 μm was observed for the hydrogels, and the macroporous architectures were similar. The PB10 hydrogels displayed an interconnected and irregular porous morphology, with the largest pore size (average: 82 μm) among the four hydrogel formulations. The addition of HLC and the higher-molecule-weight pullulan resulted in a relatively increased crosslinking density in the hydrogel structure, and the PBH10 and PBH53 hydrogels appeared to have a more compact porous structure, with an average pore size ranging from 55 to 69 μm. Evidently, due to the higher crosslinking density, the pore partitions of the PBH53 hydrogels were the thickest. The particle morphologies are illustrated in Fig. 3 (C: particles). In particular, homogeneous particles were observed, and the particle morphology was similar to the structure of the hydrogels, except that the particles were circular. A porous structure with interconnected open pores was evidently obtained from the particles after lyophilization.

Fig.2

Fig. 2. Visual observation of PB and PBH hydrogels and the swelling behavior and BDDE residual in four hydrogels: (A) PB10 hydrogels; (B) PBH10 hydrogels; (C) PB53 hydrogels; (D) PBH53 hydrogels; (E) freeze-dried hydrogels; (F) freeze-dried hydrogels re-dissolved for 48 h; (G) freeze-dried hydrogels re-dissolved for 96 h; (H) hydrogels granulated into particles and distilled at 121°C for 5 min, four times; (I) four particle types filled into a 1-mL syringe for injection; (E1) the swelling ratio of the four hydrogels in deionized water; (F1) the length of the four hydrogels during the swelling process; (G1) the diameter of the four hydrogels during the swelling process; (H1) BDDE residual in the four hydrogels.

3.3 Enzymatic degradation of the PB and PBH hydrogels

The effect of HLC and the pullulan molecular weight on the

susceptibility of the PB and PBH hydrogels towards enzymatic digestion was evaluated using an *in vitro* enzymatic degradation assay. The four hydrogels were incubated in the presence of pullulanase, collagenase I and pullulanase/collagenase I at 37°C. The enzymatic reactions were stopped at different times after the retrieval of the wet hydrogels. The morphologies of the hydrogels were observed after enzymatic degradation, as shown in Fig. 3 (D: pullulanase, E: collagenase I and F: pullulanase/collagenase I). SEM images of the degraded hydrogels confirmed a collapse of the substrate structure by the combination of pullulanase/collagenase I degradation at the microscopic level, while the porous three-dimensional architecture was preserved for all of the hydrogels after treatment with pullulanase or collagenase I. The restriction enzyme site of pullulanase is the α-1, 6-glycosidic bond (Fig. 4 A (P)), and the site for collagenase I is the hydroxyPro-Leu-Gly-Pro-Ala peptides (Fig. 4B (C)). Therefore, the molecular weight of the hydrogels was lower after degradation. However, for the combination of the two enzymes, the weight decreased rapidly. As a result, the morphology of the hydrogels was completely changed after degradation by pullulanase/collagenase I. The weight loss was also determined by weighing the dry hydrogels after degradation (Fig. 4 C, D and E).

Fig.3

Fig. 3. Cross-sections of the PB and PBH hydrogels before and after degradation by pullulanase, collagenase I and pullulan/collagenase I, as observed by SEM. The first line denotes the cross-section for the four hydrogels (50 ×), with a scale bar of 400 μm; the second line represents the cross-section for the four hydrogels at a higher magnification (100 ×), with a scale bar of 200 μm; the third line represents the particles for the four hydrogels (100 ×), with a scale bar of 200 μm; the fourth line denotes the cross-section for the four hydrogels after degradation by pullulanase (100 ×), with a scale bar of 200 μm; the fifth line represents the cross-section for the four hydrogels after degradation by collagenase I (100 ×), with a scale bar of 200 μm; the sixth line denotes the cross-section for the four hydrogels after degradation by pullulanase/collagenase I (250 ×), with a scale bar of 100 μm.

Different stages were identified in the *in vitro* degradation behavior of the hydrogels. In the first stage, between 0 and 3 weeks, the degradation exhibited various physical phenomena, including mimicking the body temperature, simulating body fluid, mechanical behavior, and releasing other degradation products in the solution, such as high-MW polymeric chains. After 3 weeks, there was an unexpected decrease in the molecular weight. The MW of the hydrogels decreased continuously with degradation time, resulting in significant weight loss. For longer immersion times, the registered changes in the weight were less significant. Eventually, the MW of the gels decreased to a low value, which remained nearly unchanged with time; this lack of change was related to the degradation of the hydrogel matrix.

Fig.4

Fig. 4. The molecular structure of the PB hydrogels (A) and PBH hydrogels (B) during degradation by pullulanase and collagenase I. Weight loss observed for the PB and PBH hydrogels after degradation by pullulanase (C), collagenase I (D) and pullulanase/collagenase I (F).

It is generally believed that enzyme involvement is likely in the early degradation stages for pullulan chains and HLC. Previous investigations have indicated that enzymatic biodegradation primarily occurs on the hydrogel surface because it is difficult for non-hydrophilic enzymes to diffuse into a hydrophobic polymer [21], while enzymatic biodegradation of the hydrogels involves hydrolysis of the hydrogel chain backbone. Additionally, it is expected that the surface area of the hydrogels would have a strong influence on enzymatic degradation. Therefore, when the PB10 and PB53 hydrogels were degraded by collagenase I, the weight loss was higher than in PBH10 and PBH53; thus, the hydrogel surface influences the mechanical behavior. Similar results were reported by Mochizuki et al. [22] Because the mechanical behavior of hydrogels is very sensitive to degradation, an understanding of the relevant mechanisms and their control will allow for the production of materials with the appropriate mechanical performance for temporary biomedical applications.

3.4 Mechanical strength of the PB and PBH hydrogels

The relationship between the compression load and compression displacement of the wet hydrogels is shown in Fig. 5 A and B. The four wet hydrogels present different mechanical behaviors after 6 mm of compression. Under maximum stress, PBH10 experienced fracture indication, while the other hydrogels did not fracture under maximum compression. Compared with wet PBH10, the wet PBH53 with intense structure have lower water content which lead to the weaker ability against compression. The compression load of wet PBH53 (0.035MPa) is lower than wet PBH10 (0.07 MPa). According to the modulus varies positively correlated with compression load. Therefore, the modulus of wet PBH53 is lower than wet PBH10. In a similar way, the modulus of wet PB53 is lower than wet PB10. However, compared with wet PB10 and PB53, the wet PBH10 exhibited a relatively high elastic module at 0.2 MPa (Fig. 5 B'). It's mainly due to the crack during compression displacement from 5.5-6mm.

Functional hydrogels can be used for cartilage repair or lacrimal dryness therapy. The mechanical strength, as one of the important character for cartilage or lachrymal duct, was measured in our dry hydrogels study. The bending stresses of the four dry hydrogels also demonstrated different behaviors (Fig. 5 C'). Due to the three-dimensional structure, the bending stress attained a maximum value of 1600 MPa for the crosslinkers and HLC. For the PBH hydrogels, the abrupt increase in mechanical strength likely resulted from an increase in chemical crosslinkage or physical entanglement. Apparently, for the dry PBH hydrogels, the HLC crosslinking with pullulan was optimal for achieving the highest elastic modulus, with a maximum value of 7858.93 MPa (Fig. 5D'). Under compression, stress in the dry PB hydrogels can easily develop locally inside the network, leading to the formation of cracks. However, the presence of a soft but loose network of PBH hydrogels could effectively dissipate the stress imposed during compression by deforming the network conformation (Fig. 5 C and D). Furthermore, the compression behaviors of the four dry hydrogels also differed (Fig. 5 E'). The compression modulus of the dry hydrogels was higher than that of the wet hydrogels for the same compression displacement (Fig. 5F').

Fig.5

Fig. 5. The mechanical behavior of the PB and PBH hydrogels. (A') The wet hydrogels were subjected to compressional stress using an Electronic

Universal Testing Machine. (A and B) The relationship between compression load and compression displacement for the four wet hydrogels. (B') The elastic modulus of wet PB hydrogels and PBH hydrogels. (C') The bending stress of dry hydrogels, determined using an Electronic Universal Testing Machine. (C and D) The relationship between bending stress and compression displacement for the four dry hydrogels. (D') Elastic modulus of dry PB hydrogels and PBH hydrogels. (E') The compression stress of dry hydrogels, as measured by an Electronic Universal Testing Machine. (E, F, G and H) The relationship between compression load and compression displacement for the four dry hydrogels. (F') Elastic modulus of dry PB hydrogels and PBH hydrogels. (G') Pore size for the four hydrogels.

An elastic hydrogel subjected to a relatively small deformation (less than 20%) fully recovers its original dimensions, thus justifying an analysis of the meshwork structure based on the rubber-elasticity theory. [23] Applying this theory extends the aforementioned correlation between stiffness (i.e., elastic modulus) and the crosslinking density (i.e., the number of covalently bonded chains of pullulan-HLC) to estimate the average pore size of the networks. Assuming that all of the chains contribute to the retraction force after deformation in a similar way (affine deformation), neglecting the end effects of individual chains (all chains have fixed ends towards an elastic background), and excluding any influence of physical entanglement, the following equation was used to evaluate the mesh size ξ of the gels (affine network model): [24]

$$\xi = (GN_A/RT)^{-1/3}$$

where G is the elastic modulus, N_A is Avogadro's constant, R is the molar gas constant, and T is the temperature. The mesh size of the gels was found to be at the micron scale. Decreasing mesh sizes of 82 µm (PB10), 75 µm (PB53), 69 µm (PBH10), and 55 µm (PBH53) were found for materials with increasing pullulan MW and following the addition of HLC (Fig. 5 G'). The increased crosslinking density resulted in a denser network that was more rigid (higher elastic modulus) and that exhibited restricted water uptake due to the larger reaction forces caused by the higher number of covalent bridges within the gel (decreased swelling). These findings reflect nearly ideal elastic behavior for these materials and demonstrate the stability of the network obtained through the covalent crosslinkage. Furthermore, this result allows for a more detailed investigation of the network structure.

3.5 Cell adhesion and live/dead staining

A major challenge in tissue engineering is to obtain controlled or desired cell adhesion under physiological conditions through optimized surface characteristics, as cell adhesion influences subsequent cell events such as proliferation and cell viability. [25] We examined the ability of PB and PBH hydrogels with different molecular weights to support cell viability and cell adhesion. Fibroblasts were seeded on the surfaces of the hydrogels and allowed to attach for 24 and 72 h; the gels were then washed with PBS to remove any unattached cells. Cell viability studies were performed for the cells seeded on the hydrogels using a live/dead staining. In Fig.6, SEM results indicated that the four hydrogels supported cell attachment, while the cell morphologies were significantly different. The cell attachment and growth rates were much higher on PBH10, with cell elongation and integration, and some cells actively contracted onto the hydrogels. The cell morphology also differed in this case. In contrast, cell attachment, migration and spreading were observed on the other hydrogels, leading to a round cell morphology and a low proportion of contracting. This difference was attributed to the rigidity of the crosslinked higher-molecular-weight pullulan and HLC. As shown in Fig. 7 A, B, C and D, the cells remained viable with few dead cells, the death rate is 25%, 15%, 12% and 11%, respectively. Image analysis using live/dead staining showed a significantly higher number of cells attached on the PB10 and PB53 hydrogels compared with the PBH10 and PBH53 hydrogels. The PB10 and PB53 hydrogels exhibited more cytotoxicity, with many dead cells on the surfaces and a cell viability of 70% and 80%. However, the PBH10 and PBH53 hydrogels showed lower cytotoxicity, with few dead cells on the surface and a cell viability higher than 86% and 85%.

Fig.6

Fig. 6. Cell adhesion adherent cells on the hydrogels. SEM images of fibroblast attachment on the PB10 hydrogel (A1, A2, and A3), PBH10 hydrogel (B1, B2, and B3), PB53 hydrogel (C1, C2, and C3) and PBH53 hydrogel (D1, D2, and D3) at 24 (A1, B1, C1 and D1), 48 (A2, B2, C2 and D2) and 72 h (A3, B3, C3 and D3); the scale bar is 10 µm.

Given that the BDDE-modified hydrogels also support cell adhesion and spreading, our results indicate that the BDDE-modified hydrogels showed a favorable cell response. We hypothesize that this result is due to the intermixing of HLC and pullulan, which altered the physicochemical properties of the hydrogel surface to render it cell adhesive. Indeed, surface hydrophilicity, hydration and swelling, as well as surface roughness, are considered to be important for cell attachment. [26] As discussed previously, the addition of HLC decreased the swelling of the PBH hydrogels and considerably modified their roughness. Based on the SEM images (Fig. 3), an increased surface roughness was observed on the PB10 and PB53 hydrogels. However, the HLC chain crosslinking with pullulan indicated an increased surface hydrophobicity, which correlates well with the increased cell attachment. Altogether, our data suggest that the presence of HLC promotes cell adhesion and spreading on the hydrogel surface, making PBH hydrogels more suitable for tissue engineering.

Fig.7

Fig. 7. Evaluation of fibroblast live/dead staining. Fibroblast were cultured on the PB10 hydrogels (A, E), PBH10 hydrogels (B, F), PB53 hydrogels (C, G) and PBH53 hydrogels (D, H) and control group with live/dead staining at 1 (A, B, C and D) and 3 days (E, F, G and H). Scale bar for all images: 200 µm. The death rates were shown in histogram in 1 and 3days.

3.6 H&E staining

Fig. 8 show the hydrogels and surrounding tissue stained by H&E. The *in vitro* enzyme response study produced promising results, while the degradation of the hydrogels *in vivo* was attributed to tissue-responsiveness, resulting in non-sustained degradation. The hydrogels presented here were designed to inhibit degradation in a sustained and tissue-dependent manner, and the biocompatibility of the substrate was determined by a decrease in inflammation cells and inflamed tissue after 24 weeks. These hydrogels are a promising candidate for minimally invasive degradation as they can be polymerized using HLC modification and higher-MW pullulan.

Fig.8

Fig. 8. H&E staining of PB and PBH hydrogels and the surrounding tissue in rabbits. PB10 hydrogels (A, E), PBH10 hydrogels (B, F), PB53 hydrogels (C, G) and PBH53 hydrogels (D, H) were subcutaneously injected into rabbits at 1 (A, B, C and D) and 24 weeks (E, F, G and H). G presents the hydrogels. Scale bar for all images: 2 mm.

3.7 Inflammation of injectable hydrogels in mice and rabbits

Having demonstrated that the PB and PBH hydrogels can induce enhanced cell adhesion in vitro, we studied the in vivo inflammation response in Kunming mice (Fig. 9) and rabbits (Fig. 10). We selected different subcutaneous positions on the Kunming mice for comparison (Fig. 9 I and II). Fig. 9I shows results for the four particle types subcutaneously injected at the same position on the back of the mice, indicating that the four particle types led to different inflammation responses. The inflammation cells exhibited different morphologies after a reaction between the tissue and the particles at 1 and 24 weeks. We selected physiological saline as a control group was shown in Fig.9 (A-1, B-1 and C-1). The control group showing that spinal cells in the granular layer and a large number of collagen fibers with spindle-shaped fibroblasts. Fig. 9 I (1 week) shows that macrophages, fibroblasts, lipid droplets, collagen fibers, endoplasmic reticulum and blood vessels were observed. The PB hydrogels produced few fibroblasts and a large number of collagen fibers, with vertical and horizontal alternations in the tissue; the PBH particles produced few macrophages, a large number of collagen fibers and an expansion of the endoplasmic reticulum. After 24 weeks (Fig. 9 I (24 weeks)), the PB and PBH particles produce few macrophages, a larger number of collagen fibers and a large expansion of the endoplasmic reticulum. The above data suggest that the response of the PB and PBH particles to inflammation in the Kunming mice tissue decreased after 24 weeks, resulting in almost normal tissue. In contrast, the responses of the four particle types at the different positions also produced low degrees of inflammation; the cells had returned to their original shape by the end of the experiment (Fig. 9 II (24 weeks)).

To further evaluate the therapeutic filler efficacy of the PBH and PB particles, New Zealand rabbits were used as a model. It has been reported that rabbits are more sensitive to the surrounding tissue than Kunming mice and even more than human skin. Fig. 10 displays the efficiency of the four hydrogels for the surrounding tissue of each rabbit. In Fig. 10 A, B, C and D at 1 and 24 weeks, it is shown that with for pullulan with a higher molecular weight, the subcutaneously filled particles decreased the vascular swelling. However, with the addition of HLC, the PBH particles adapted more to the rabbit's skin tissue and gradually increased the ability of tissue adsorption. From these observations, it is clear that the conjugation of active polymer and HLC occurs efficiently and that the composition of the materials is optimal for the conjugation of the activations of HLC, resulting in the formation of skin.

Fig.9

Fig. 9. Biocompatibility of the PB and PBH hydrogels *in vivo*. The hydrogels were subcutaneously injected at the same position (I) and at different positions (II) on the back of Kunming mice. (I 1 week and 24 weeks) TEM images are shown with a magnification of 5000× (for A, B, C, D, E, F, G and H, the scale bar is 5 μm). Images with a magnification of 10000× (for E1, F1, G1 and H1, the scale bar is 2 μm) are shown for the PB10, PBH10, PB53 and PBH53 hydrogels at the site surrounding the mice tissue for 1 and 24 weeks. (II 1 week and 24 weeks) TEM images are shown at a magnification of 10000× (scale bar for all images: 2 μm) for the PB10, PBH10, PB53 and PBH53 hydrogels at the site surrounding the tissue for 1 and 24 weeks. The numbers represent the following: 1, macrophages; 2, fibroblasts; 3, collagen fibers; 4, lipid droplets; 5, endoplasmic reticulum; 6, blood vessels; 7, spinal cells.

To determine whether the rabbit skin affinity is reduced due to the modification of pullulan with HLC, an *in vivo* test was conducted using TEM (Fig. 10). The data confirm that the modification of pullulan did not adversely affect the inflammation response at 1 week. The four particles interact with the surrounding tissue and produce few macrophages, fibroblasts and collagen fibers; a large number of lipid droplets (LDs) were observed in the PB10 and PBH10 particles. It has been demonstrated that LDs promote an increase in lipolysis in adipocytes. [27] At 24 weeks after injection, the number of macrophages and fibroblasts and the endoplasmic reticulum size had returned to approximately the initial state. From the above results, it is clear that the inflammation response of the PBH particles is capable of maintaining higher anti-inflammation levels than the PB particles in rabbits. Our animal experiments thus indicate a possible therapeutic role for these particles as skin fillers and even as substitutes for cartilage.

Conclusions

A series of novel skin fillers with HLC backbones and non-ionic pullulan chains with different molecular weights were successfully prepared via crosslinking with BDDE. Pullulan chains with various MWs were readily crosslinked by BDDE under alkaline conditions. Due to the epoxidation reaction and the Schiff base reaction, the PBH hydrogels exhibited a much higher elastic modulus and enhanced cell adhesion, cell viability, anti-biodegradation and anti-inflammation in comparison to the PB hydrogels. Particularly, in comparison with the lower-MW PBH10, PBH53 exhibited excellent compatibility with rabbits and mice without causing inflammation and resulted in a degradation time longer than 6 months. Importantly, these wet hydrogels can be readily prepared as particles to restore tissue, and freeze-dried hydrogels can be readily restored to their original state in deionized water to replace cartilage due to their superior elastic behavior. The *in vivo* results for the PB and PBH particles are promising, and this process can provide a safe system for subcutaneous injections in mice and rabbits. The mechanical strength and enzymatic degradation of the PB and PBH hydrogels were established under *in vitro* conditions, and preliminary experiments showed promising results for therapeutic applications. Thus, proper functionalization of an HLC backbone with higher-MW chains of pullulan provides a unique means for designing a new class of biocompatible and efficient hydrogels and particles for tissue engineering.

Fig.10

Fig. 10. Biocompatibility of the PB and PBH hydrogels *in vivo*. (A, B, C and D) The rabbits were sacrificed, and the hydrogel and periphery tissue were carefully removed 1 (I) and 24 (II) weeks after injection. 5000× TEM images (A1, B1, C1, D1, A2, B2, C2 and D2; the scale bar is 5 μm) and 10000× TEM images (A3, B3, C3 and D3; the scale bar is 2 μm) of PB10 (A, A1, A2 and A3), PBH10 (B, B1, B2 and B3), PB53 (C, C1, C2 and C3) and

PBH53 (D, D1, D2 and D3) hydrogels at the site surrounding the mice tissue at 1 (I) and 24 (II) weeks. The numbers represent the following: 1, macrophages; 2, fibroblasts; 3, collagen fibers; 4, lipid droplets; 5, endoplasmic reticulum; 6, blood vessels.

Acknowledgements

This study was financially supported by the National Natural Science Foundation of China (21476182); the National High Technology Research and Development Program of China (2014AA02108); the Scientific Research Program of Shannixi Provincial Department of Education, China (14JS102); and the Scientific and Technologic Research Program of Shaanxi Province Academy of Sciences, China (No. 2014k-01).

Notes and references

[1]*Shaanxi Key Laboratory of Degradable Biomedical Materials, Department of Chemical Engineering, Northwest University, Taibai North Road 229, Xi'an, Shaanxi 710069, China*
[2]*Shannxi provincial institute of microbiology, xi' an 710043, China*
* Corresponding author: Tel.: +86- 29-88305118; Fax: +86-29-88322585
E-mail address: fandaidi@nwu.edu.cn (D. D. Fan)
§ These authors contributed equally to this work

1 X. C. Yang, Y. L. Niu, N. N. Zhao, C. Mao, F. J. Xu, *Biomaterials*, 2014, **35**, 3873; G. Fundueanu, M. Constantin, I. Oanea, V. Harabagiu, P. Ascenzi, B. C. Simionescu, *Biomaterials*, 2010, **31**, 9544; M. R. Rekha, K. Pal, P. Bala, M. Shetty, I. Mittra, G. S. Bhuvaneshwar, C. P. Sharma, *Biomaterials*, 2013, **34**, 6328.
2 S. Tanodekaew, M. Prasitsilp, S. Swasdison, B. Thavornyutikarn, T. Pothsree, R. Pateepasen , *Biomaterials*, 2004, **25**, 1453.
3 X. Li, X. X. Ma, D. D. Fan and C. H. Zhu, *Soft Matter*, 2012, **8**, 3781-3790; X. Li, X. X. Ma, D. D. Fan and C. H. Zhu, *Soft Materials*, 2014, **12**, 1.
4 M. Ishihara, K. Obara, T. Ishizuka, M. Fujita, M. Sato, K. Masuoka, Y. Saito, et al, *J Biomed Mater Res*, 2003, **64**A, 551; D. K. Kweon, S. B. Song, Y. Y. Park , *Biomaterials*, 2003, **24**, 1595; J. F. Keuren, S. J. Wielders, G. M. Willems, et al, *Biomaterials*, 2003, **24**, 1917.
5 M. Leonard, D. Rastello, M. Boisseson, P. Hubert, E. Dellacherie, J Biomed Mater Res, 2003, **68**A, 335; A. Perets, Y. Baruch, F. Weisbuch, G. Shoshany, G. Neufeld, S. Cohen, *J Biomed Mater Res*, 2003, **65**A, 489; F. S. Kamelger, R. Marksteiner, E. Margreiter, G. Klima, G. Wechselberger, S. Hering, H. Piza, *Biomaterials*, 2004, **25**, 1649.
6 G. Fundueanu, M. Constantin, I. Oanea, V. Harabagiu, P. Ascenzi, B. C. Simionescu, *Biomaterials*, 2010, 31, 9544; H. Yim, S. G. Yang, Y. S. Jeon, *Biomaterials*, 2011, **32**, 5187.
7 M. R. Rekha, C. P. Sharma, *Biomaterials*, 2009, **30**, 6655.
8 J. C. Fricain, S. Schlaubitz, C. L. Visage, et al, *Biomaterials*, 2013, **34**, 2947.
9 Y. S. Wang, H. L. Chen, Y. Y. Liu, et al, *Biomaterials*, 2013, **34**, 7181.
10 C. H. Zhu, D. D. Fan, Z. G. Duan, W. J. Xue, L. A. Shang, *J Biomed Mater Res Part A*, 2009, **89**(A), 829.
11 P. M. Santos, J. G. Winterowd, G. G. Allen, M. A. Bothwell, and E. W. Rubel, *Head Neck Surg*, 1991; **105**, 12.
12 Y. Y. Yu, D. D. Fan, *SpectrochimicaActa Part A*, 2011, **81**, 412.
13 X. Li, X. X. Ma, D. D. Fan and C. H. Zhu, *Journal of Materials Chemistry B*, 2014, **2**, 1234.
14 L. Wang, J. P. Stegemann, *Acta Biomater*, 2011, **7**, 2410.
15 M. Jastrzebska, J. Zalewska-Rejdak, R. Wrzalik, A. Kocot, B. Barwinski, I. Mróz, B. Cwalina, *J Mol Struct*, 2005, **744**, 789.
16 S. Ibrahim, C.R. Kothapalli, Q.K. Kang, A. Ramamurthi, *Acta Biomater*, 2011, **7**, 653.
17 V. Maier, C. M. Lefter, S. S. Maier, et al., *Materials Science and Engineering C*, 2014, **42**, 243.
18 A Raza, C.S. Ki, C.C. Lin. *Biomaterials*, 2013, **34**, 5117.
19 J. K. Xu, S. Strandman, X. X. Zhu, J. Barralet, M. Cerruti, *Biomaterials*, 2015, **37**, 395.
20 H. Park, X. Guo, J. S. Temenoff, Y. Tabata, A. I. Caplan, F. K. Kasper, et al., *Biomacromolecules*, 2009, **10**, 541; S. Woerly, S. Fort, I. Pignot-Paintrand, C. Cottet, C. Carcenac, M. Savasta, *Biomacromolecules*, 2008, **9**, 2329.
21 A. J. Kuijpers, *J. Biomater . Sci. P olymer Edn*, 2000, **11**(3), 225.
22 M. Mochizuki, M. Hirano, Y. Kanmuri, K. Kudo, Y. Tokiwa, *J Appl Polym Sci*, 1995, **55**, 289.
23 M. Rubinstein, R. H. Colby, Polymer physics. Oxford, New York: Oxford University Press; 2003.
24 G. P. Raeber, M. P. Lutolf, J. A. Hubbell, *Biophys J*, 2005, **89**, 1374.
25 S. Yamanlar, S. Sant, T. Boudou, C. Picart, A. Khademhosseini, *Biomaterials*, 2011, **32**, 5590.
26 L. Richert, F. Boulmedais, P. Lavalle, J. Mutterer, E. Ferreux, G. Decher, et al., *Biomacromolecules*, 2004; **5**(2), 284.
27 A. S Greenberg , W. J. Shen , K. Muliro , S. Patel , S. C. Souza , R. A. Roth , F. B. Kraemer, *J. Biol. Chem*, 2001, **276**, 45456; H. H. Zhang, M. Halbleib, F. Ahmad, V. C. Manganiello, A. S. Greenberg, *Diabetes*, 2002, **51**, 2929.

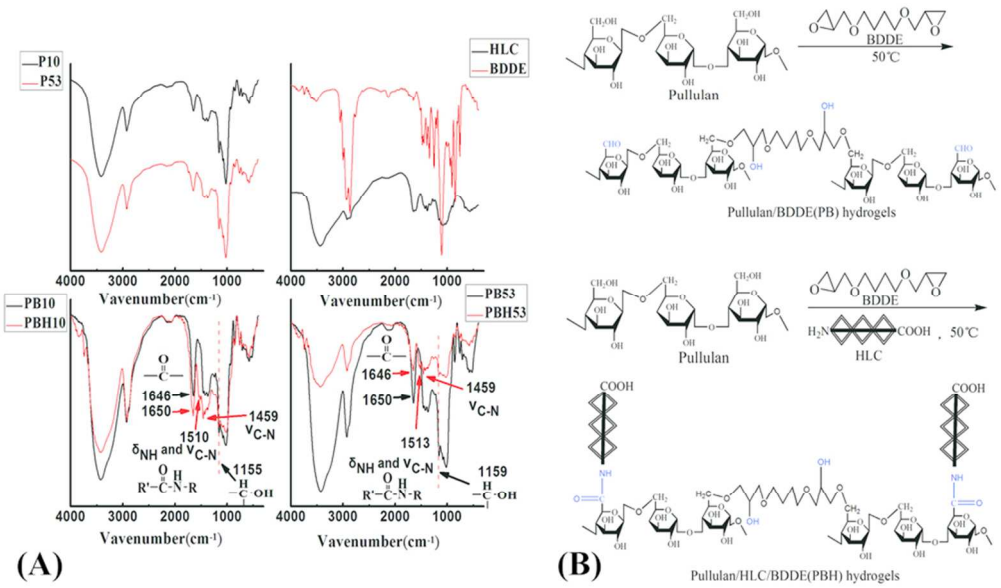

Fig. 1. (A) FT-IR spectra of P10, P53, HLC, BDDE, PB10, PBH10, PB53 and PBH53. (B) Proposed mechanisms for interactions among pullulan, HLC and BDDE: the reaction among pullulan, HLC and BDDE in a hot bath at 50°C under alkaline conditions.
85x50mm (300 x 300 DPI)

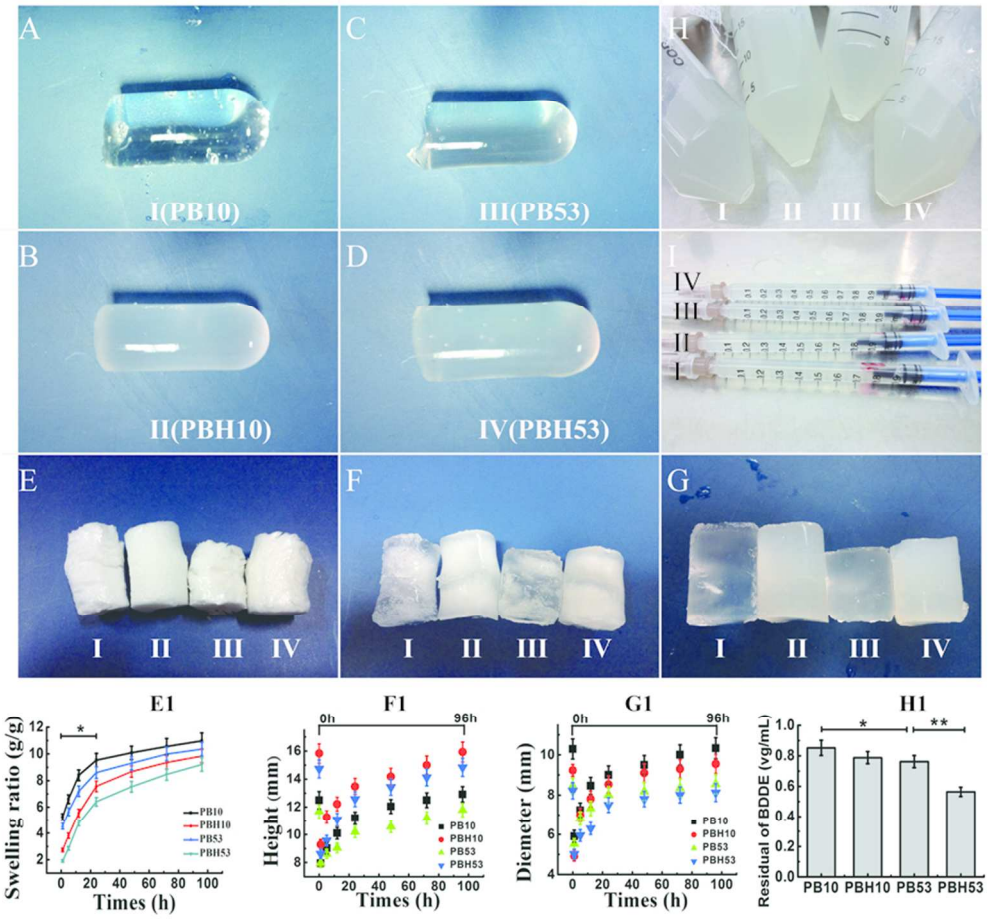

Fig. 2. Visual observation of PB and PBH hydrogels and the swelling behavior and BDDE residual in four hydrogels: (A) PB10 hydrogels; (B) PBH10 hydrogels; (C) PB53 hydrogels; (D) PBH53 hydrogels; (E) freeze-dried hydrogels; (F) freeze-dried hydrogels re-dissolved for 48 h; (G) freeze-dried hydrogels re-dissolved for 96 h; (H) hydrogels granulated into particles and distilled at 121°C for 5 min, four times; (I) four particle types filled into a 1-mL syringe for injection; (E1) the swelling ratio of the four hydrogels in deionized water; (F1) the length of the four hydrogels during the swelling process; (G1) the diameter of the four hydrogels during the swelling process; (H1) BDDE residual in the four hydrogels.
80x74mm (300 x 300 DPI)

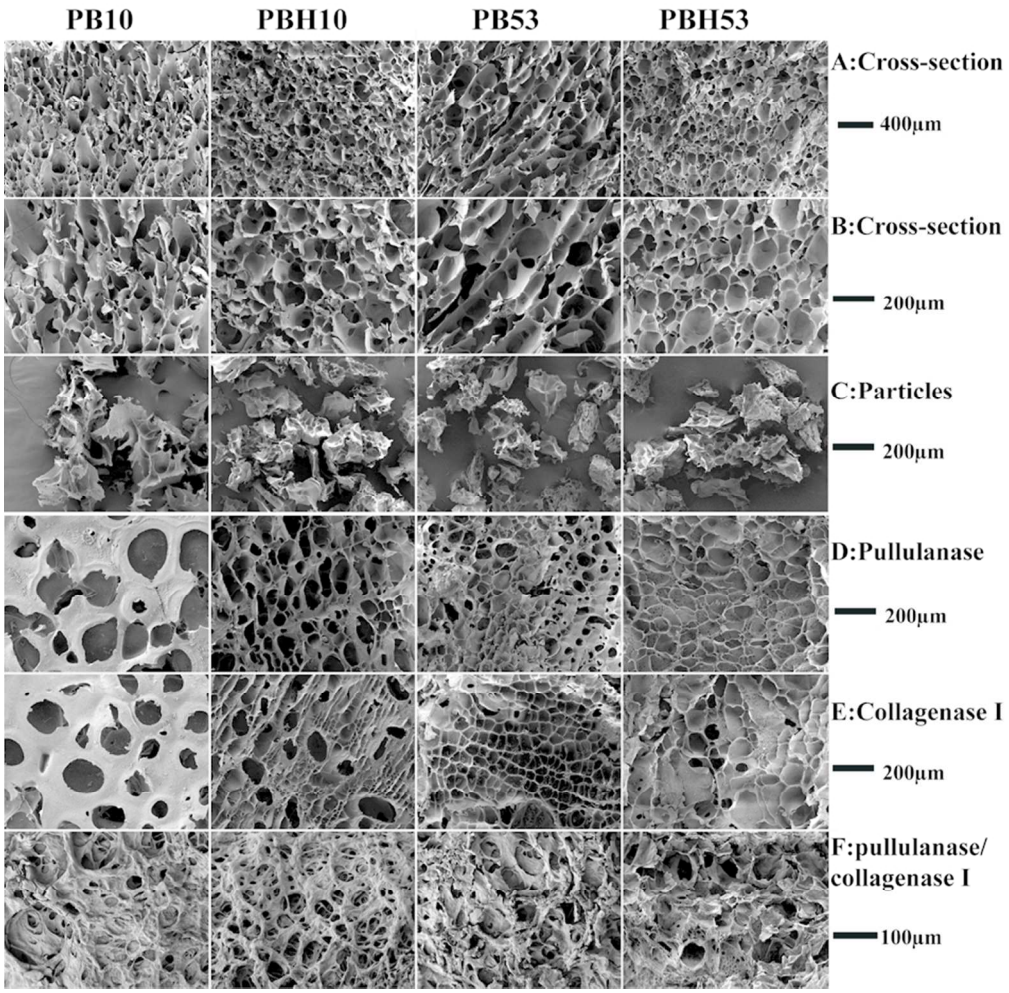

Fig. 3. Cross-sections of the PB and PBH hydrogels before and after degradation by pullulanase, collagenase I and pullulan/collagenase I, as observed by SEM. The first line denotes the cross-section for the four hydrogels (50 ×), with a scale bar of 400 μm; the second line represents the cross-section for the four hydrogels at a higher magnification (100 ×), with a scale bar of 200 μm; the third line represents the particles for the four hydrogels (100 ×), with a scale bar of 200 μm; the fourth line denotes the cross-section for the four hydrogels after degradation by pullulanase (100 ×), with a scale bar of 200 μm; the fifth line represents the cross-section for the four hydrogels after degradation by collagenase I (100 ×), with a scale bar of 200 μm; the sixth line denotes the cross-section for the four hydrogels after degradation by pullulanase/collagenase I (250 ×), with a scale bar of 100 μm.
80x78mm (300 x 300 DPI)

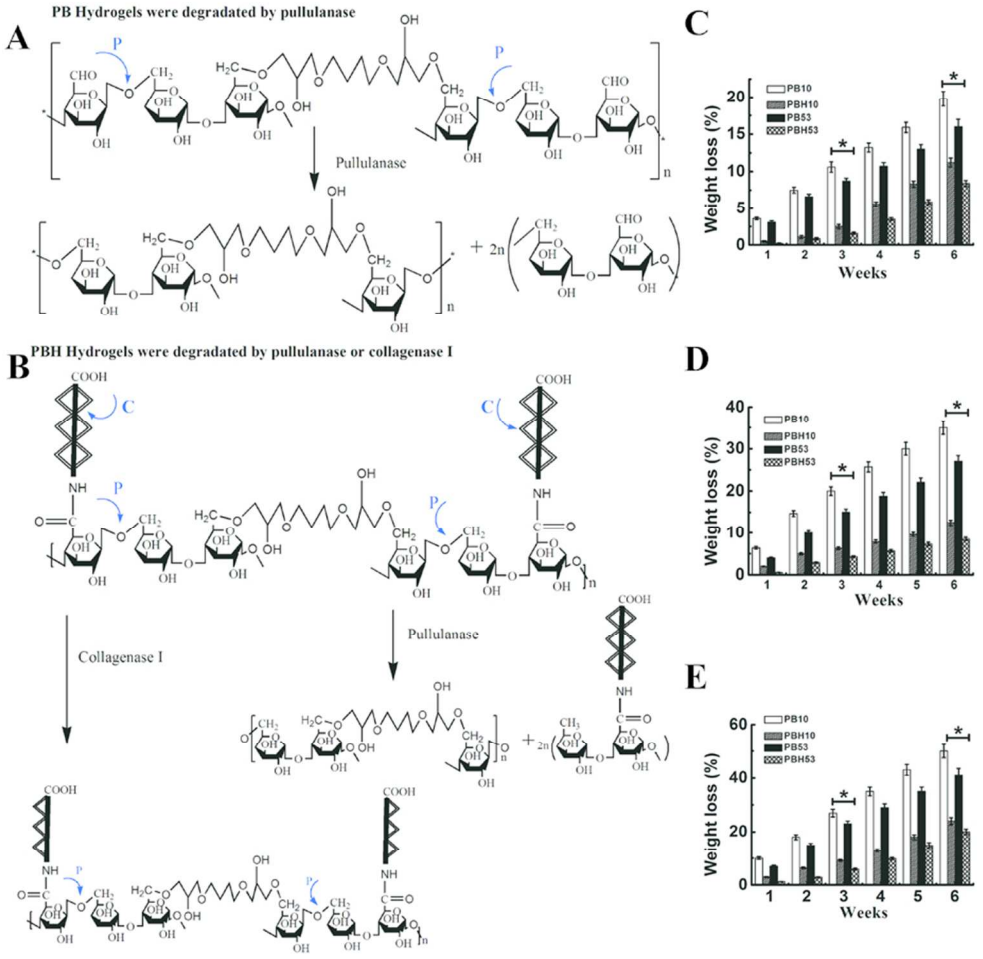

Fig. 4. The molecular structure of the PB hydrogels (A) and PBH hydrogels (B) during degradation by pullulanase and collagenase I. Weight loss observed for the PB and PBH hydrogels after degradation by pullulanase (C), collagenase I (D) and pullulanase/collagenase I (F).
80x76mm (300 x 300 DPI)

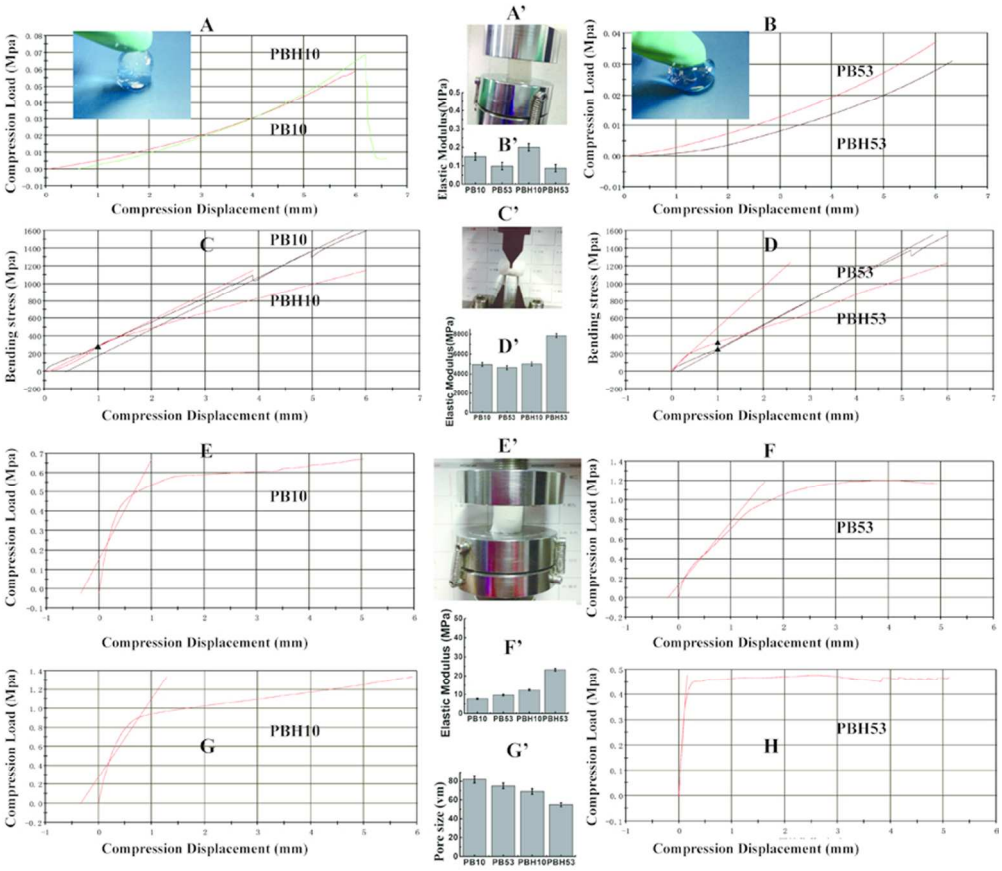

Fig. 5. The mechanical behavior of the PB and PBH hydrogels. (A') The wet hydrogels were subjected to compressional stress using an Electronic Universal Testing Machine. (A and B) The relationship between compression load and compression displacement for the four wet hydrogels. (B') The elastic modulus of wet PB hydrogels and PBH hydrogels. (C') The bending stress of dry hydrogels, determined using an Electronic Universal Testing Machine. (C and D) The relationship between bending stress and compression displacement for the four dry hydrogels. (D') Elastic modulus of dry PB hydrogels and PBH hydrogels. (E') The compression stress of dry hydrogels, as measured by an Electronic Universal Testing Machine. (E, F, G and H) The relationship between compression load and compression displacement for the four dry hydrogels. (F') Elastic modulus of dry PB hydrogels and PBH hydrogels. (G') Pore size for the four hydrogels.
80x69mm (300 x 300 DPI)

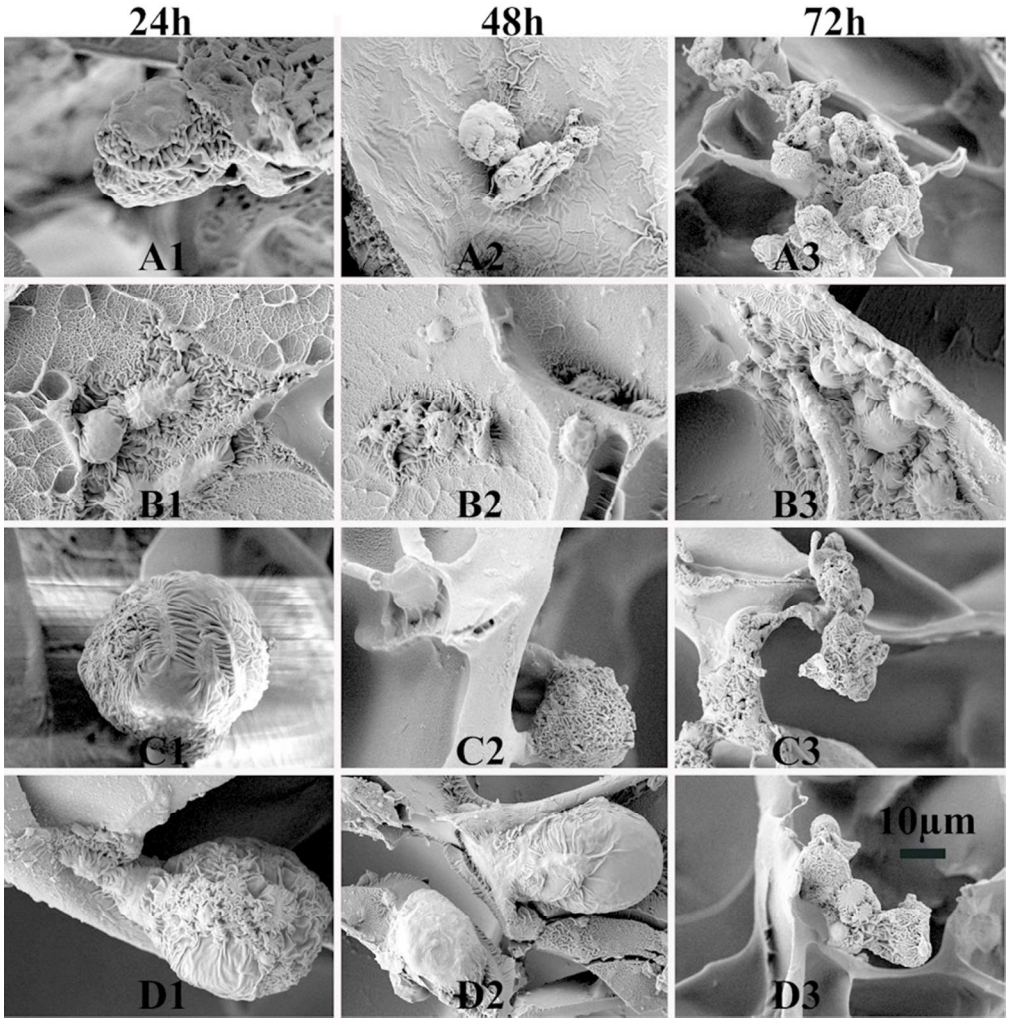

Fig. 6. Cell adhesion adherent cells on the hydrogels. SEM images of fibroblast attachment on the PB10 hydrogel (A1, A2, and A3), PBH10 hydrogel (B1, B2, and B3), PB53 hydrogel (C1, C2, and C3) and PBH53 hydrogel (D1, D2, and D3) at 24 (A1, B1, C1 and D1), 48 (A2, B2, C2 and D2) and 72 h (A3, B3, C3 and D3); the scale bar is 10 μm.
80x82mm (300 x 300 DPI)

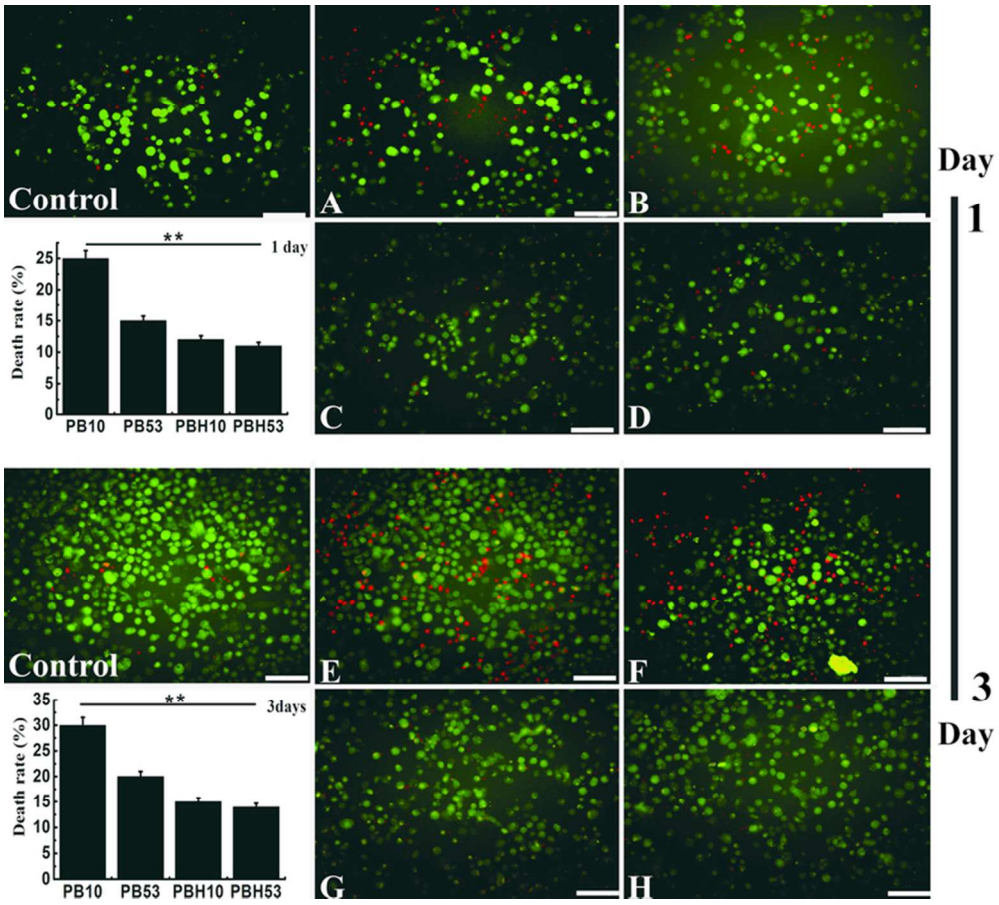

Fig. 7. Evaluation of fibroblast live/dead staining. Fibroblast were cultured on the PB10 hydrogels (A, E), PBH10 hydrogels (B, F), PB53 hydrogels (C, G) and PBH53 hydrogels (D, H) and control group with live/dead staining at 1 (A, B, C and D) and 3 days (E, F, G and H). Scale bar for all images: 200 μm. The death rates were shown in histogram at 1 and 3days.
71x63mm (300 x 300 DPI)

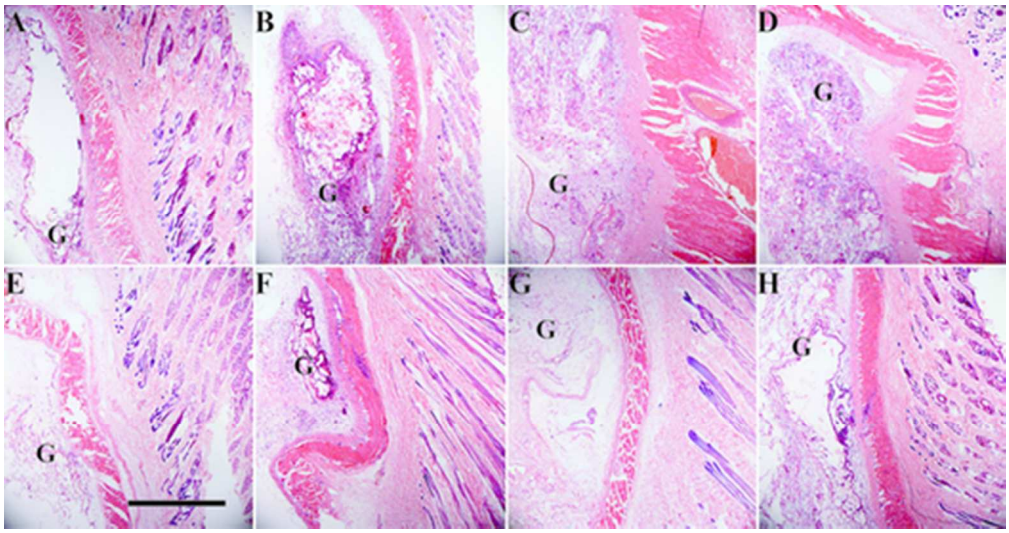

Fig. 8. H&E staining of PB and PBH hydrogels and the surrounding tissue in rabbits. PB10 hydrogels (A, E), PBH10 hydrogels (B, F), PB53 hydrogels (C, G) and PBH53 hydrogels (D, H) were subcutaneously injected into rabbits at 1 (A, B, C and D) and 24 weeks (E, F, G and H). G presents the hydrogels. Scale bar for all images: 2 mm.
44x23mm (300 x 300 DPI)

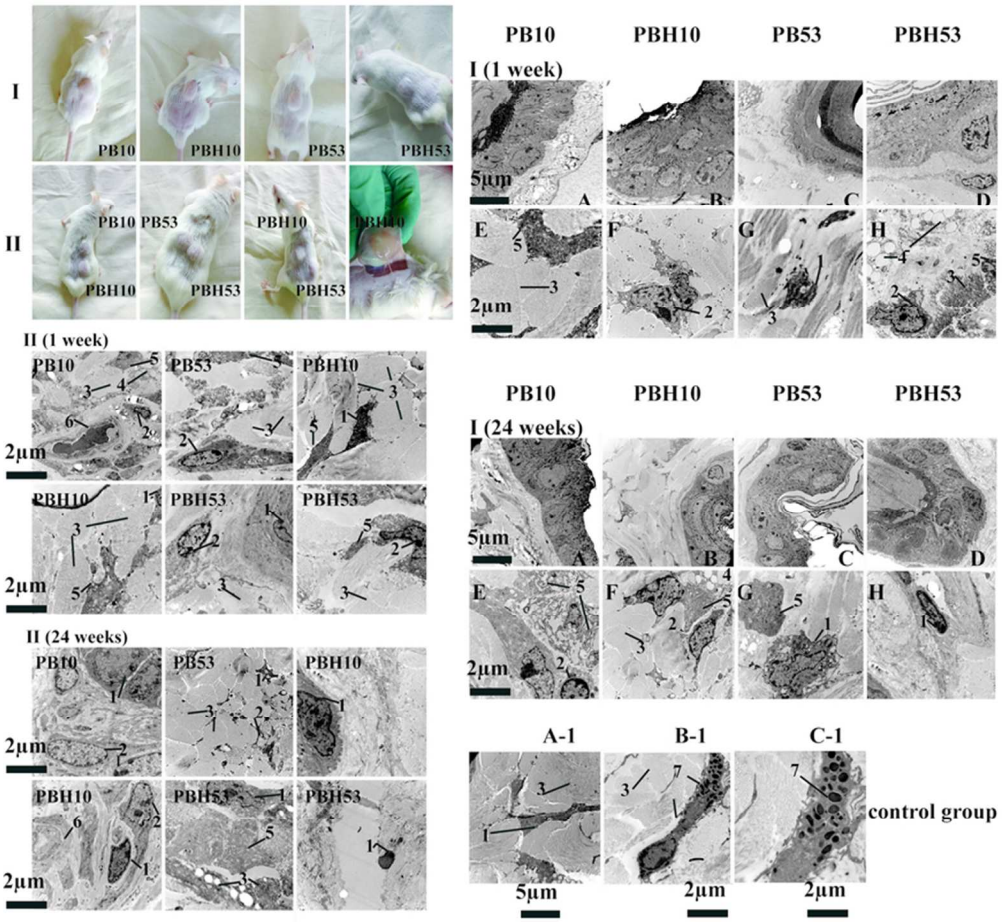

Fig. 9. Biocompatibility of the PB and PBH hydrogels in vivo. The hydrogels were subcutaneously injected at the same position (I) and at different positions (II) on the back of Kunming mice. (I 1 week and 24 weeks) TEM images are shown with a magnification of 5000× (for A, B, C, D, E, F, G and H, the scale bar is 5 μm). Images with a magnification of 10000× (for E1, F1, G1 and H1, the scale bar is 2 μm) are shown for the PB10, PBH10, PB53 and PBH53 hydrogels at the site surrounding the mice tissue for 1 and 24 weeks. (II 1 week and 24 weeks) TEM images are shown at a magnification of 10000× (scale bar for all images: 2 μm) for the PB10, PBH10, PB53 and PBH53 hydrogels at the site surrounding the tissue for 1 and 24 weeks. The numbers represent the following: 1, macrophages; 2, fibroblasts; 3, collagen fibers; 4, lipid droplets; 5, endoplasmic reticulum; 6, blood vessels; 7, spinal cells.
73x67mm (300 x 300 DPI)

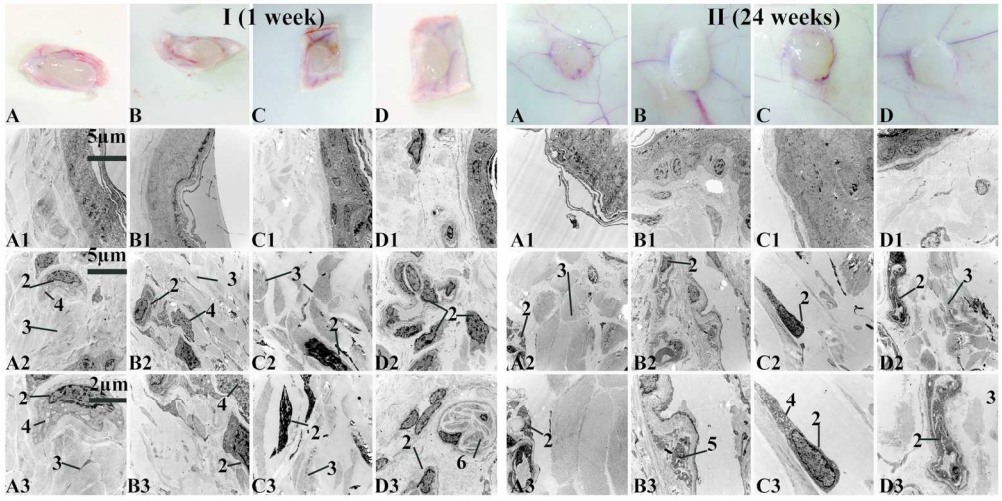

Fig. 10. Biocompatibility of the PB and PBH hydrogels in vivo. (A, B, C and D) The rabbits were sacrificed, and the hydrogel and periphery tissue were carefully removed 1 (I) and 24 (II) weeks after injection. 5000× TEM images (A1, B1, C1, D1, A2, B2, C2 and D2; the scale bar is 5 μm) and 10000× TEM images (A3, B3, C3 and D3; the scale bar is 2 μm) of PB10 (A, A1, A2 and A3), PBH10 (B, B1, B2 and B3), PB53 (C, C1, C2 and C3) and PBH53 (D, D1, D2 and D3) hydrogels at the site surrounding the mice tissue at 1 (I) and 24 (II) weeks. The numbers represent the following: 1, macrophages; 2, fibroblasts; 3, collagen fibers; 4, lipid droplets; 5, endoplasmic reticulum; 6, blood vessels.
170x84mm (300 x 300 DPI)

Abstract graphical

The multifunctionalized hydrogel (PB and PBH hydrogels) scaffolds and injectable particles with good biocompatibility, cell adhesion, higher mechanical strength and anti-biodegradation are based on high-molecular-weight (MW) pullulan and human-like collagen (HLC) crosslinked with 1, 4-butanediol diglycidyl ether (BDDE) for combination therapy tissue restoration, such as skin restoration, cartilage treatment, and lacrimal dryness therapy.